Desalination and Water Treatment
www.deswater.com
doi: 10.5004/dwt.2019.23351

137 (2019) 183–193
January

MgFe compounds for water purification: the effect of annealing temperature on lead removal performance

Tik Lun Leung[a,*], Chun Sing Kam[a], Qian Sun[a], Aleksandra B. Djurišić[a], Mao Hai Xie[a], Wai Kin Chan[b], Hang Kong Li[c], Ying Zhou[c], Kaimin Shih[c]

[a]*Department of Physics, The University of Hong Kong, Pokfulam, Hong Kong, Tel. +85228592528; emails: u3005505@connect.hku.hk (T.L. Leung), kcsj9000@gmail.com (C.S. Kam), lilysqq@gmail.com (Q. Sun), dalek@hku.hk (A.B. Djurišić), mhxie@hku.hk (M.H. Xie)*
[b]*Department of Chemistry, The University of Hong Kong, Pokfulam, Hong Kong, email: waichan@hku.hk (W.K. Chan)*
[c]*Department of Civil Engineering, The University of Hong Kong, Pokfulam, Hong Kong, emails: hangkong@connect.hku.hk (H.K. Li), zhouy223@connect.hku.hk (Y. Zhou), kshih@hku.hk (K. Shih)*

Received 25 May 2018; Accepted 24 October 2018

ABSTRACT

Co-precipitation in alkaline solution is a straightforward synthesis method for layered double hydroxide (LDH) materials. Iron-containing LDH materials readily transform to spinel ferrite upon annealing. We prepared MgFe compounds annealed at different temperatures and investigated the effect of annealing temperature on their physical properties and lead adsorption abilities. The co-precipitated samples annealed at 400°C and 600°C exhibited LDH crystal structure, while the samples annealed at 700°C and 800°C had spinel ferrite structure. The maximum lead adsorption capacity reduced with increasing annealing temperature. Transformation from MgFe LDH to spinel ferrite structure after annealing at 600°C leads to the loss of surface area and the elimination of interlayer anions, resulting in a reduction of lead adsorption capacity. Although decreased lead adsorption capacity was found in spinel ferrite sample, magnesium leaching was significantly reduced compared with MgFe LDH samples, indicating enhanced sample stability.

Keywords: Layered double hydroxide; Spinel ferrite; Lead removal; Magnesium leaching

1. Introduction

Significant environmental pollution with a range of pollutants harmful to human health, such as dyes, pesticides, pharmaceuticals, heavy metals, etc., has resulted in increasing demand for clean water. Therefore, there is a rising interest in the development of materials for water purification, including various metal oxides and their composites, spinel ferrites, and layered double hydroxides (LDH) [1–33]. Inorganic pollutants, such as arsenic, cadmium, chromium, lead, mercury and selenium, are of significant interest since they can have adverse health effects even at trace concentrations [2,3]. In addition, they have relatively low adsorption affinity for commonly used adsorbent materials, such as activated carbon. Lead is a commonly occurring major inorganic environmental pollutant, mainly due to industrial wastewater containing lead-acid battery residues [2,5,6]. Since lead is known to cause severe health complications, such as neurological problems, anemia, liver and kidney issues, cancer and death [2], there is significant interest in the development of efficient adsorbent materials for lead removal.

Among different adsorbent materials, spinel ferrites have been attracting increasing attention [1–14,21] due to their desirable properties, such as high performance and the ease of separation. Spinel ferrite materials share some common

* Corresponding author.

characteristics with more extensively studied iron oxide-based materials [15,17–20], such as being environmentally benign and having low cost, while they can exhibit better stability [1]. They have a general formula of MFe_2O_4, where M is a divalent metal such as Mn, Co, Cu, Ca, Zn, Mg, etc. [1]. Spinel ferrites, mainly Zn, Ni, Mn, Co, and Cu ferrites [2], have been extensively studied for wastewater treatment and the removal of various pollutants, such as metal ions (including Pb^{2+}), dyes, and organic pollutants [1]. Compared with other spinel ferrites, $MgFe_2O_4$ has been less studied [1,2], despite its high stability, non-toxicity and cost-efficiency [10]. It has been investigated for the adsorption of organic dyes [1,11], phosphate [10], chromium [1], arsenic [1], cobalt [1,11] and lead [1,9,21].

LDH materials represent another class of materials of high interest for contaminant removal [22–33]. LDH materials have a general formula $[M^{2+}_{1-x}\ M^{3+}_{x} \times (OH)_2]^{x+}\ (A^{n-})_{x/n} \times mH_2O$, where M^{2+} is the divalent metal, M^{3+} is the trivalent metal, A^{n-} is the charge compensating interlayer anion, and *m* is the number of water molecules [22,23]. They have been used for the removal of lead [22–24,26,27,29,30,32,33], chromium [25,28], copper [29,31], nickel [33], zinc [33], cadmium, halides and oxyanions [29]. Similar to spinel ferrites, MgFe LDH materials [26,30,33] have been less studied compared with LDH compounds with other compositions, such as MgAl LDH.

While LDH and spinel ferrites are both of interest for lead adsorption, there has been no direct comparison of their performance. Nevertheless, it is well known that iron-containing LDH compounds can transform into spinel ferrites upon annealing. In addition, annealing temperature can affect various factors related to adsorption properties, such as particle morphology and surface adsorbates [1]. Therefore, here we investigate the lead adsorption performance of MgFe compounds annealed at different temperatures to elucidate the effects of morphology, properties, and transformation from MgFe LDH into magnesium ferrite on lead adsorption. We also investigated their chemical stability (in terms of Fe and Mg leaching) and compared the performance to the MgO and Fe_2O_3 mixture. We found that MgFe LDH materials had higher lead adsorption capacity compared with $MgFe_2O_4$, while magnesium ferrite exhibited lower leaching out of magnesium compared with both MgFe LDH and a mixture of MgO and Fe_2O_3. Obtained results are discussed in detail in the following.

2. Experimental

2.1. Synthesis of MgFe compounds

MgFe compounds were prepared by co-precipitation method followed by calcination at different temperatures. Briefly, 10 mmol iron (III) chloride and 30 mmol magnesium nitrate hexahydrate were dissolved in 10 mL water. The solution was then precipitated in 10 mL alkaline solution of 20 mmol sodium carbonate and 10 mmol sodium hydroxide under stirring. The obtained precipitate was washed with water and ethanol thrice, and dried at 80°C under vacuum. Finally, the powder was annealed at 400°C, 600°C, 700°C and 800°C, and these samples are labeled as MF400, MF600, MF700 and MF800, respectively. MgO/Fe_2O_3 composite was prepared by direct mixing of MgO and Fe_2O_3 with 1:1 molar ratio. MgO nanoparticles with size 10–30 nm were purchased from Skyspring, while Fe_2O_3 was prepared according to a previously reported procedure [34].

2.2. Characterization

Crystal structures of MgFe compounds were analyzed by X-ray diffraction (XRD) using a Bruker D8 Advance Diffractometer with Cu Kα radiation (λ = 0.154184 nm). Material morphologies were characterized by scanning electron microscopy (SEM) using a Hitachi S-4800 FEG Scanning Electron Microscope. In addition, high resolution transmission electron microscopy (HRTEM) images and selected area electron diffraction (SAED) patterns of the samples were obtained using a FEI Tecnai G2 20 S-TWIN Scanning Transmission Electron Microscope. Thermogravimetric analysis (TGA) was performed from 30°C to 600°C at heating rate 10°C/min. using a Q50 Thermal Gravimetric Analyzer. N_2 isotherms of different samples were measured by Quantachrome Quadrasorb EVO Analyzer at 77 K, and the pore size distribution was calculated by Barrett–Joyner–Halenda model in desorption branch. Fourier transform infrared spectra (FTIR) were collected from a pellet containing the sample and KBr using a PerkinElmer Spectrum Two IR Spectrometer. X-ray photoelectron spectra (XPS) were measured using EscaLAB 205 Xi XPS system equipped with Al Kα X-ray source.

2.3. Lead adsorption testing

Stock metal ion solutions of 1,000 ppm were prepared from nitrate salt and desired concentrations were prepared via dilution from stock. Isotherm studies were performed by dispersing 10 mg sample in 10 mL lead solution of 10, 25, 100, 250 and 500 ppm. Solution pH was in the range 7.5–8.0 for all concentrations after adding the MgFe samples. After 6 h, solutions were passed through 0.22 μm syringe filter. For kinetic adsorption studies, 50 mg of each sample was added into 50 mL lead solution with the concentration of 50 ppm (solution pH was 5.8 before adding MgFe samples). The filtrates were collected at desired time (every minute for first 5 min, then at 10 and 15 min). For pH dependent lead adsorption experiment, pH was adjusted to a desired value by adding 0.01 M HCl and NaOH solutions. Lead, iron, nickel, copper, zinc and magnesium contents in the collected solution were measured using an Optima 8000 ICP-OES Spectrometer (PerkinElmer).

3. Results and discussion

Fig. 1 shows the XRD patterns of different samples. Significant differences can be observed in samples annealed at lower temperatures (MF400 and MF600), compared with samples annealed at higher temperatures (MF700 and MF800). The samples annealed at lower temperatures exhibit diffraction peaks in good agreement with those corresponding to MgFe LDH with CO_3^- as the interlayer anion [35]. The LDH phase was further confirmed by SAED and HRTEM, shown in Supplementary Information, Fig. S1. On the other hand, all the observed peaks in MF700 and MF800 samples correspond to $MgFe_2O_4$ (JCPDS #88-1935). MgO and Fe_2O_3 samples exhibit good crystallinity, with observed peaks

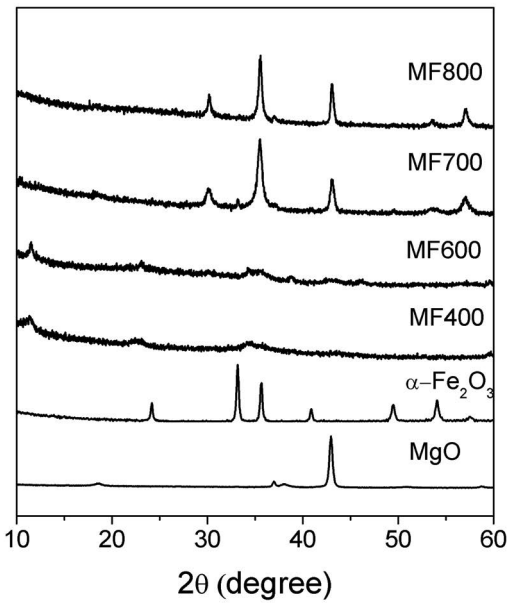

Fig. 1. X-ray diffraction patterns of different samples.

in good agreement with reported values for MgO (JCPDS #45-0946) and α-Fe_2O_3 (JCPDS #01-089-8103).

From the SEM images of the samples (Supplementary Information, Figs. S2 and S3), we can observe that annealing does not result in a significant change in morphology of the particles with the same crystal structure, i.e. we can observe similarities between MF400 and MF600 (LDH samples), and MF700 and MF800 (spinel ferrite samples). Some reduction in particle aggregation can be observed when comparing MF400 and MF600 samples, while the particle size is the largest for MF800 samples. A significant increase in particle sizes is observed upon transition from MgFe LDH to $MgFe_2O_4$. This is in agreement with the estimate of crystallite sizes obtained from XRD results. Based on Scherrer's equation [6,7,36], the crystallite sizes can be estimated. From the (003) peak of LDH samples, we can estimate crystallite sizes of 8.9 and 21.7 nm for MF400 and MF600, respectively, while for $MgFe_2O_4$ samples from (220) peak we can estimate crystallite sizes of 23.4 and 64.3 nm for MF700 and MF800, respectively. It should also be noted that the particle sizes for binary oxides (MgO, Fe_2O_3) are significantly smaller compared with magnesium ferrite or MgFe LDH. In addition to morphology and crystal structure characterization by XRD and electron microscopy, the surface areas and pore structures were characterized by N_2 adsorption–desorption analysis (Fig. S4). The surface areas of MF400, MF600, MF700 and MF800 are measured to be 185.62, 65.46, 34.17 and 12.79 m^2/g, respectively. The total pore volume of MF400, MF600, MF700 and MF800 measured at P/Po = 0.994 were 1.091, 0.420, 0.267 and 0.038 cm^3/g, respectively. MF400 has the highest surface area and pore volume with narrow peak at 5.95 nm (Fig. S5). N_2 isotherm results were summarized in Table S1. The reduction in the available surface area with increasing annealing temperature is in agreement with the observed morphology and crystallinity changes in SEM and XRD characterization.

From TGA measurements shown in Fig. 2, we can observe that MF400 sample exhibits the largest weight loss with increasing temperature, and that the weight loss occurs in two stages, as expected in LDH materials [37,38]. The lower temperature (up to ~170°C) weight loss corresponds to the dehydration of superficial and interlayer water, while the higher temperature weight loss (>220°C) corresponds to dehydroxylation and decarbonation processes [37,38]. Weight loss in the samples annealed at higher temperature is significantly smaller, in agreement with a previous report on thermally activated MgAl LDH annealed at 550°C [38]. Small weight loss in MgO + Fe_2O_3 mixture and MF700 samples corresponds to the loss of the surface adsorbates, while MF800 samples exhibit negligible weight loss up to 600°C. From the XPS results (Supplementary Information, Figs. S6 and S7), we can observe relevant peaks in C1s, O1s, Mg 1s and Fe 2p regions. The most significant differences between MgFe LDH samples and $MgFe_2O_4$ can be observed in the C 1s and O 1s spectra, which is likely due to the presence of interlayer carboxyl ions in LDH samples. In the C 1s spectrum, peaks at 284.8, 286.3 and 288.8 eV can be attributed to C-C, C-O, and C=O, respectively [21]. In MgFe LDH samples, four peaks in C1s region were previously reported, with peaks at 284.6 and 285.3 eV assigned to C-H and C-C bonds [33] or to C-C (284.1 eV) and C=C (284.9 eV) [30], respectively, while the two higher energy peaks were assigned to C-O and C=O [30,33], similar to $MgFe_2O_4$ samples [21]. The O1s peak contains peaks corresponding to lattice oxygen at ~529.9 eV, metal hydroxide or surface hydroxyl groups at ~531.8 eV [21]. For Mg, a single weak peak with binding energy of 1,304.8 eV was previously reported for $MgFe_2O_4$ [21]. The peaks at ~710.5 and 724.2 eV correspond to Fe $2p_{3/2}$ and Fe $2p_{1/2}$, respectively, while a satellite line at ~718.5 eV corresponds to Fe^{3+} [21].

To investigate the performance of different samples for lead removal, adsorption isotherms and kinetic data were measured. Different models can be used to fit the lead adsorption isotherm data [1,3–6,10,11,16,17,23,32]. Here we examined two commonly used models, namely Langmuir model and Freundlich model, which allow us to distinguish between adsorption on homogeneous (uniform binding energy) and heterogeneous (different sites with several adsorption energies) surfaces [4,6]. In a commonly

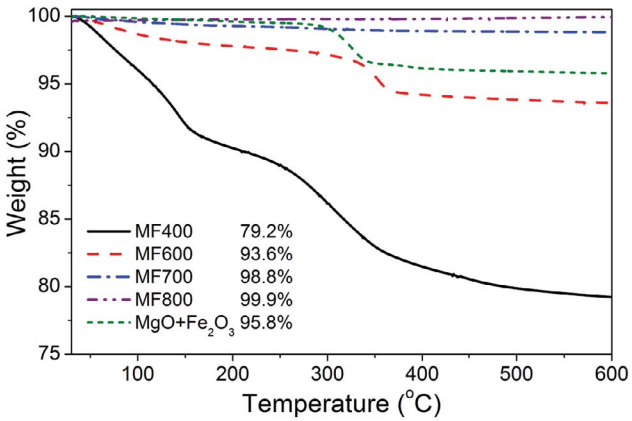

Fig. 2. Thermogravimetric analysis curves of different samples.

used Langmuir model, monolayer adsorption with uniform binding energy and without interactions between the adsorbed species is assumed [1,3–6,17,20,23]. Under these assumptions, the quantity of adsorbed species is given as [1,3,5,6,10,17,20,21,23]:

$$q_e = q_m K_L \frac{C_e}{1 + K_L C_e} \quad (1)$$

This linear form of this equation can be approximated as [4–6,20,32]:

$$\frac{C_e}{q_e} = \frac{1}{q_m K_L} + \frac{C_e}{q_m} \quad (2)$$

Another common isotherm model is a Freundlich model. This is an empirical model developed for describing a heterogeneous surface containing different sites with several adsorption energies, and the quantity of adsorbed species is given as [1,3,5,6,10,11,17,23]:

$$q_e = K_F C_e^{1/n} \quad (3)$$

This equation can be fitted directly or rewritten to a linear form for fitting [4–6,32]:

$$\ln q_e = \ln K_F + \frac{1}{n} \ln C_e \quad (4)$$

In addition, we considered another model for the isotherms, which allows determination of the nature of the adsorption (chemisorption vs. physisorption), namely Dubinin–Radushkevich (D–R) model [5,11,16,23]. The linearized form of D–R model is [5,11,23]:

$$\ln q_e = \ln q_m - \beta F^2 \quad (5)$$

where q_m is the maximum absorption capacity, F is the Polanyi potential $F = RT \ln(1 + C_e^{-1})$, R is the universal gas constant and T is the temperature, while β is the constant, which is related to the free energy of adsorption $E = 1/\sqrt{2\beta}$. The E values <8 kJ/mol indicate physisorption, E > 16 kJ/mol indicates chemisorption, while intermediate E values indicate ion exchange [5,11].

Obtained fitting results for different models are given in Tables 1–3, respectively. The suitability of the model can be evaluated on the basis of obtained correlation coefficient values [3]. High correlation coefficient values obtained (R^2 in the range from 0.9710 to 0.9999) for the Langmuir model indicate that the adsorption process can be accurately described by a Langmuir model [3,20]. In contrast, the obtained correlation coefficient values for Freundlich model are significantly lower (0.8544–0.9265), indicating that the data are better described by a Langmuir model. The obtained correlation coefficient values for D–R model are even lower (0.700–0.927). This indicates the validity of the starting assumptions of the Langmuir model, namely monolayer adsorption with uniform binding energy. The obtained excellent fit using a Langmuir model is in agreement with the literature reports on other spinel ferrite materials [1,3–6,9,13,21], as well as LDH materials [27,30,32]. The obtained maximum adsorption capacity of $MgFe_2O_4$ samples for both annealing temperatures is higher than that previously reported for $MgFe_2O_4$ microspheres, which was 113.7 mg/g [21]. It is also higher than to that of reduced graphene oxide-$NiFe_2O_4$ composite (121.95 mg/g) [9]. The obtained capacity of MF800 is comparable to that of amine-functionalized magnesium ferrite nanoparticles (135.1 mg/g) [9], while the adsorption capacity of MF700 is significantly higher. For the MgFe LDH samples, obtained maximum capacity is lower than that previously reported for samples prepared using a more complex procedure from chloride precursors [26]. On the other hand, MF400 exhibits higher adsorption capacity compared with MgFe LDH (178.6 mg/g) and MgFe LDH with N-doped carbon hydrogel (344.8 mg/g) prepared from nitrate precursors [30]. In addition, the obtained capacity is higher than previously reported co-precipitated MgFe-LDH (317.9 mg/g) [33], but lower than that of MgFe-LDH – rice husk ash composite [33]. Also, higher adsorption capacity is obtained compared with an Mg-Al LDH (298.5 mg/g) [32]. The obtained capacity of MgO:Fe_2O_3 mixture is higher than that previously reported Fe_2O_3 (53.1 mg/g) [17], Fe_3O_4 (52.9 mg/g) [15], and slightly lower compared a previous report for MgO-graphene oxide composite (190 mg/g) [16].

Table 1
Fitting parameters and correlation coefficient values for Langmuir model

Sample	q_m (mg/g)	K_L (L/mg)	R^2
MF400	490.4	0.318	0.9928
MF600	254.9	0.546	0.9999
MF700	231.4	0.124	0.9710
MF800	136.1	0.090	0.9943
MgO + Fe_2O_3	158.1	0.165	0.9993

Table 2
Fitting parameters and correlation coefficient values for Freundlich model

Sample	K_f	n	R^2
MF400	81.33	1.80	0.9096
MF600	54.48	2.80	0.8544
MF700	49.11	3.42	0.8753
MF800	20.69	2.83	0.9265
MgO + Fe_2O_3	36.96	3.60	0.8753

Table 3
Fitting parameters and correlation coefficient values Dubinin–Radushkevich model

Sample	q_m (mg/g)	E (kJ/mol)	R^2
MF400	222.8	2.718	0.844
MF600	161.3	2.976	0.880
MF700	151.9	3.454	0.927
MF800	73.0	1.787	0.700
MgO + Fe_2O_3	121.5	1.089	0.907

We can observe that the maximum adsorption capacity of our MgFe compounds decreases as the annealing temperature increases, in agreement with a significant reduction in surface area. Annealing at lower temperatures was reported to result in higher adsorption capacity since it typically results in high surface area, surface defects and residual organic groups [1]. Thus, obtained results are in agreement with expected behaviour. We can also observe that the maximum adsorption capacity of $MgFe_2O_4$ at lower annealing temperatures exceeds that of MgO + Fe_2O_3 mixture. In addition, there is some correlation between weight losses determined by TGA and the maximum adsorption capacity. Such correlation may indicate that lead adsorption of MgFe compounds is partially attributed to the interaction with surface functional groups. The fact that MF700 sample exhibits higher lead adsorption than MgO + Fe_2O_3 mixture indicates that in $MgFe_2O_4$ other adsorption mechanisms still play a significant role, as evidenced by high lead adsorption capacity of MF800 sample despite very low presence of surface adsorbates. In oxide and spinel ferrite materials, pollutant adsorption typically occurs due to surface charge of the particles and the presence of hydroxyl groups [1,2]. In an aqueous dispersion, these materials will form an outermost layer of surface hydroxyl groups due to a reaction between the water molecules and metal oxide surface [1]. In general, possible mechanisms include ion exchange, surface complexation, and interaction of weak forces, such as van der Waals forces, hydrogen bonding, dipole–dipole and π–π interactions [1,2]. In LDH materials, various mechanisms of pollutant removal can occur, such as precipitation of metal hydroxides onto the surface of LDH, surface complexation, such as bonding with surface hydroxyl groups, chelation with the functional ligand in the interlayers and isomorphic substitution, such as replacement of Mg^{2+} with a divalent metal ion, which is sterically hindered for Pb^{2+} due to a large radius difference [29]. Nevertheless, ion exchange has been identified as contribution mechanism in lead removal by MgFe LDH [30,33]. The additional possible mechanisms of pollutant removal in LDH materials likely contribute to a significantly higher lead adsorption capacity of MF400 compared with other samples.

To obtain more information about the adsorption mechanism, FTIR measurements before and after lead absorption were performed. The obtained results for MF400 and MF800 are shown in Fig. 3. In addition, we have compared the adsorption capacity of the lead removal of these samples at different pH values, and compared the pollutant removal for different divalent metals, as shown in Fig. 4. In the FTIR spectra of MgFe LFH sample MF400, several prominent features can be observed. The broad peak at ~3,400–3,800 cm^{-1} can be attributed to hydroxyl group vibrations [8], while the peak at ~1,640 cm^{-1} corresponds to the scissoring mode vibration [15,22]. The peak at ~1,380 cm^{-1} can be attributed to COO stretching [8,23,26]. The presence of this peak in MF400 samples is in agreement with the XRD data, confirming the presence of CO_3^- as the interlayer anion. The peaks in the range 400–600 cm^{-1} correspond to the Mg-O and Fe-O vibrations [10,21]. After the lead adsorption, we can observe changes in the peak intensities and/or peak shifts in the region corresponding to metal-oxygen bond, hydroxyl group and carboxylic group, which are indicators

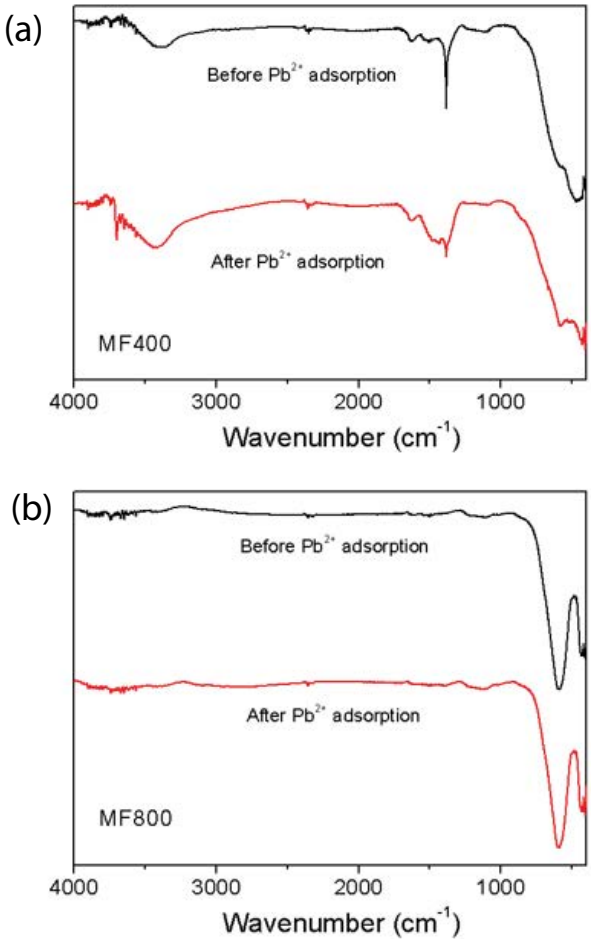

Fig. 3. Fourier transform infrared spectra spectra of MgFe oxide before and after lead adsorption. (a) MF400 and (b) MF800.

of interaction between Pb^{2+} and different surface groups [8,26]. Shift of the peak corresponding to OH vibrations is observed, in agreement with the previous report [26]. In addition, the weakening of the peak at ~1,380 cm^{-1} after the lead adsorption is consistent with the complexation of the metal with the carboxylic group [8]. Thus, FTIR spectra of LDH sample MF400 indicate clear interaction between Pb^{2+} and the surface groups present in the samples. Different from LDH samples, we can observe that the surface of MF800 magnesium ferrite does not contain significant adsorbates, with the lack of significant features corresponding to the hydroxyl group and water molecule vibrations, which are clearly observable in the LDH sample MF400. However, hydroxyl groups would be present on the sample surface in aqueous dispersion [1]. No significant change is observed in the peaks at ~588 and ~431 cm^{-1}, which correspond to the Fe-O and Mg-O vibrations [8,10–12]. The lack of significant changes in the FTIR spectrum of MF800 before and after Pb adsorption indicates that physisorption is the likely mechanism of Pb^{2+} removal, similar to a previous report on chromium adsorption on $NiFe_2O_4$ [2]. The low E values obtained from D–R model are also consistent with physisorption [5,16], although it should be pointed out that the correlation coefficient values for this model are low, and

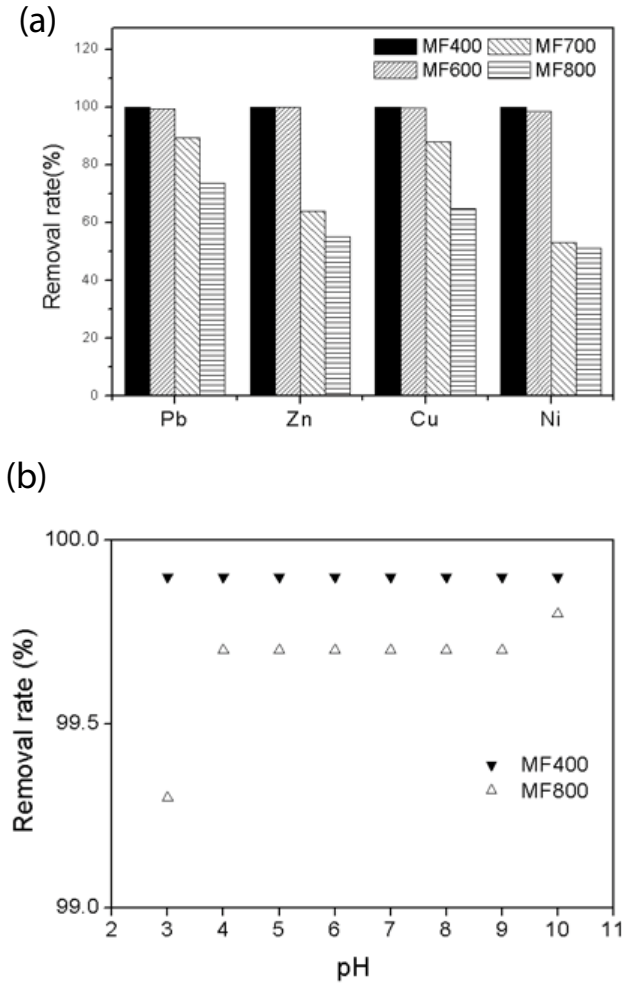

Fig. 4. (a) Competitive metal ion adsorption of mixture of Pb^{2+}, Zn^{2+}, Cu^{2+} and Ni^{2+} solution [Conc. of each ion = 10 ppm; dosage = 1 mg/ml]. (b) Influence of pH on the adsorption of metal ion [Pb^{2+} conc = 10 ppm; dosage = 1 mg/ml].

hence it does not represent a good description of the experimental data.

The obtained information from the FTIR spectrum is in agreement with the XPS results. For MF400, we observed shift in OH vibrations and significant change in the C=O vibration in FTIR spectra, while in XPS spectra we observed significant changes in the C1s and O1s peaks in MF400 after lead adsorption. The alteration of shape of C1s and O1s peaks in the XPS spectra indicates alteration of bonding environments upon Pb adsorption, including possible formation of carbonyl or carboxyl complexes, which indicates involvement of the surface groups in the Pb adsorption [30,33]. In addition, we observe a shift in the Mg peak and the reduction in intensity and the change of shape in the Fe peak (disappearance of the satellite peak corresponding to Fe^{3+}), which indicate possible ion exchange. Thus, the obtained results are in agreement with previous report, indicating that surface functional group complexation contributes to the lead removal by MgFe LDH, in addition to ion exchange process [30,33]. The ion exchange resulted in Mg leaching [33], which will be discussed in the following. For MF800 samples, much smaller changes are observed, in agreement with the FTIR results and the lower adsorption capacity. There are no significant changes in the shape of Fe 2p spectra, there is a small shift in Mg 1s peak (smaller than that of MF400 sample), small changes in C 1s spectrum, with the most significant difference observed in the shape of O 1s spectrum at higher binding energies (surface hydroxyl groups). This indicates that lead adsorption mechanisms can include physisorption, as well as possible involvement of surface water/hydroxyl groups and a small contribution of ion exchange mechanism.

From the pH dependence of the lead removal shown in Fig. 4(a), we can observe that MF400 samples exhibit stable performance over a wide range of pH values. The reduction in the lead removal at lower pH and increase at a higher pH for MF800 sample likely occurs due to the change of the surface charge of the samples since the spinel ferrites are expected to be positively charged at low pH and negatively charged at higher pH [1]. Unlike amine-functionalized $MgFe_2O_4$ nanoparticles, which exhibit high lead adsorption (>90%) only in the pH range 4–6 [9], our samples exhibited a significantly wider range of stable performance for higher pH values. Furthermore, it can be observed that MgFe spinel ferrite material MF800 exhibited better selectivity compared with MgFe LDH (MF400), as shown in Fig. 4(b). The selective lead adsorption was previously reported for amine-functionalized $MgFe_2O_4$ nanoparticles [9]. The difference in the selectivity rates between our work and the previous report [9] are likely due to the absence of surface functionalization in our samples.

To further characterize the samples, we studied adsorption kinetics in addition to adsorption isotherms. Pseudo-second order kinetic model is commonly used to describe lead adsorption on spinel ferrites, various oxides, and LDH, and it is given by the following equation [1,3–6,9,17,20,21,23,24,26]:

$$\frac{t}{q_t} = \frac{1}{q_e^2 K_2} + \frac{t}{q_e} \tag{6}$$

Obtained parameters are given in Table 4. The obtained high values of the correlation coefficients (0.9893–0.9997) indicate that the samples can be described well with pseudo-second order kinetic model. Lead adsorption curves from kinetic measurements are shown in Fig. 5. The obtained K_2 values in all cases were higher than that previously reported for $MgFe_2O_4$ microspheres prepared by a hydrothermal

Table 4
Fitting parameters and correlation coefficient values for pseudo-second order kinetic model

Sample	q_e (mg/g)	K_2 (g/mg min)	R^2
MF400	50.07	0.1672	0.9997
MF600	53.03	0.0250	0.9893
MF700	54.22	0.0168	0.9978
MF800	54.94	0.0089	0.9912
$MgO + Fe_2O_3$	51.98	0.0368	0.9974

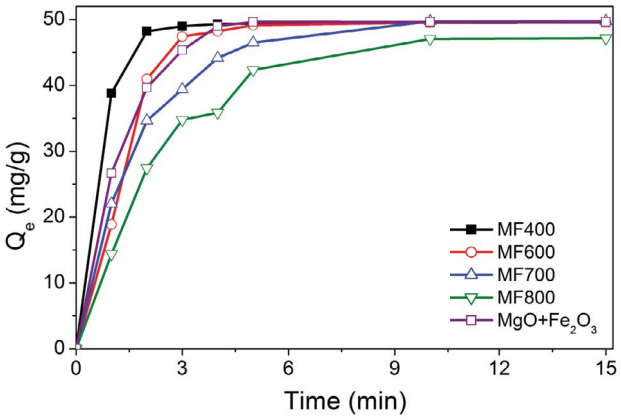

Fig. 5. Lead adsorption capacity as a function of time.

method [21]. In terms of the adsorption kinetics as well, MF400 sample exhibits superior performance compared with other samples. MF600 exhibits better performance than MF700, but this difference is much smaller compared with the difference between MF400 and MF600.

Finally, we tested whether any leaching of Fe or Mg occurred. No leaching of iron was detected under the testing conditions (iron content was below the detection limit of 0.5 ppm), similar to the previous report on MgO coated magnetite [20]. We can observe that higher Mg loss can be observed from LDH samples as well as MgO + Fe_2O_3 mixture, compared with spinel ferrite materials, as shown in Fig. 6. Leaching of Mg was previously observed in Mg-Al LDH in acidic solutions [39], MgFe LDH [33], as well as MgO-containing samples [20]. The correlation between the Mg leaching from MgO-containing samples and the lead adsorption capacity was previously observed [20]. The leaching of Mg was attributed to the ion exchange mechanism of Pb removal [20,33]. This process likely contributes to the leaching of Mg in our samples. Due to significantly lower surface area and different crystal structure, fewer Mg atoms are accessible on the surface of spinel ferrite samples compared with LDH samples, leading to less Mg leaching

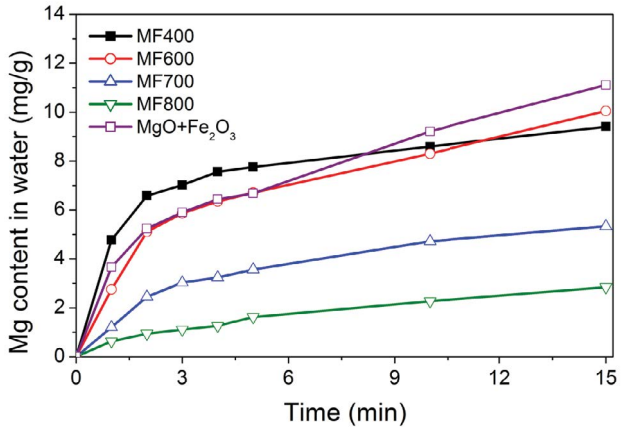

Fig. 6. Magnesium concentration as a function of time.

out of the samples. This indicates higher stability of spinel ferrite materials, which may result in improved adsorbent lifetime due to the reduced loss of Mg over time. MF700 demonstrates a good compromise between improved stability of magnesium ferrite and high lead adsorption capacity of an MgFe LDH. It should also be noted that various spinel ferrites have demonstrated good regeneration for heavy metal pollutant adsorption using acids or bases for pollutant desorption [1,2,13], while there are difficulties in the regeneration of LDH materials [33]. Spinel ferrites have high stability over a wide range of pH (pH > 3), and hence they can be readily regenerated [2,13]. However, the need for further study of stability and metal ion leaching has been pointed out [1]. We have clearly demonstrated lack of iron leaching and low Mg^{2+} leaching from our magnesium ferrite samples. Further study is needed to optimize the annealing temperature to achieve the best compromise between lead adsorption capacity and magnesium leaching, and optimize sample regeneration for practical applications, since desorption and regeneration is dependent on the properties of the adsorbent and desorbate, eluent, pH, temperature and contact time [2].

4. Conclusions

MgFe compounds for lead adsorption can be prepared by a simple co-precipitation method, and their crystal structure and lead adsorption capacity varies with the annealing temperature. Annealing at lower temperatures (400°C and 600°C) results in MgFe LDH structure with high lead adsorption capacity, but this material is susceptible to the leaching out of Mg. An increase in the annealing temperature to 700°C results in the transformation of the MgFe LDH into magnesium ferrite with comparable lead adsorption to the MgFe LDH annealed at 600°C, but significantly lower magnesium leaching from the sample. The loss of Mg is additionally reduced by increasing the annealing temperature to 800°C. However, this results in further loss of the lead adsorption capacity.

Conflicts of interest

There are no conflicts to declare.

Acknowledgement

Financial support from the Innovation and Technology Fund project ITS/366/15 is acknowledged.

Symbols

c_e	—	The equilibrium concentration of lead ion in water, mg/L
k_2	—	The rate constant of the pseudo-second order adsorption, g/mg min
K_F	—	Freundlich constant, mg/g
K_L	—	Langmuir constant, L/mg
N	—	Constant related to isotherm nonlinearity
q_e	—	The quantity of adsorbed species per quantity of sorbent material, mg/g
q_m	—	The maximum adsorption capacity per quantity of sorbent material, mg/g

q_t — The adsorption capacity per quantity of sorbent material at time t, mg/g

t — Time, s

References

[1] D.H.K. Reddy, Y.S. Yun, Spinel ferrite magnetic adsorbents: alternative future materials for water purification? Coord. Chem. Rev., 315 (2016) 90–111.

[2] K.K. Kefeni, B.B. Mamba, T.A.M. Msagati, Application of spinel ferrite nanoparticles in water and wastewater treatment: a review, Sep. Purif. Technol., 188 (2017) 399–422.

[3] L.P. Lingamdinne, J.R. Koduru, Y.L. Choi, Y.Y. Chang, J.K. Yang, Studies on removal of Pb(II) and Cr(III) using graphene oxide based inverse spinel nickel ferrite nano-composite as sorbent, Hydrometallurgy, 165 (2016) 64–72.

[4] K. Cai, W. Shen, B. Ren, J. He, S. Wu, W. Wang, A phytic acid modified $CoFe_2O_4$ magnetic adsorbent with controllable morphology, excellent selective adsorption for dyes and ultra-strong adsorption ability for metal ions, Chem. Eng. J., 330 (2017) 936–946.

[5] B. Fang, Y. Yan, Y. Yang, F. Wang, Z. Chu, X. Sun, J. Li, L. Wang, Adsorption of Pb^{2+} from aqueous solution using spinel ferrite prepared from steel pickling sludge, Water Sci. Technol., 73 (2016) 1112–1121.

[6] A.R. Vazquez-Olmos, M. Abatal, R.Y. Sato-Berru, G.K. Pedraza-Basulto, V. Garcia-Vazquez, A. Sainz-Vidal, R. Perez-Bañuelos, A. Quiroz, Mechanosynthesis of MFe_2O_4 (M=Co, Ni, and Zn) magnetic nanoparticles for Pb removal from aqueous solution, J. Nanomater., 2016 (2016) 9182024.

[7] X. Wu, W. Wang, F. Li, S. Khaimanov, N. Tsidaeva, M. Lahoubi, PEG-assisted hydrothermal synthesis of $CoFe_2O_4$ nanoparticles with enhanced selective adsorption properties for different dyes, Appl. Surf. Sci., 389 (2016) 1003–1011.

[8] Z. Zou, Z. Shi, L. Deng, Highly efficient removal of Cu(II) from aqueous solution using a novel magnetic EDTA functionalized $CoFe_2O_4$, RSC Adv., 7 (2017) 5195–5205.

[9] J. Nonkumwong, S. Ananta, L. Srisombat, Effective removal of lead(II) from wastewater by amine-functionalized magnesium ferrite nanoparticles, RSC Adv., 6 (2016) 47382–47393.

[10] K. W. Jung, S. Lee, Y. J. Lee, Synthesis of novel magnesium ferrite ($MgFe_2O_4$)/biochar magnetic composites and its adsorption behavior for phosphate in aqueous solutions, Bioresour. Technol., 245 (2017) 751–759.

[11] V. Srivastava, Y.C. Sharma, M. Sillanpää, Application of nano-magnesso ferrite (n-$MgFe_2O_4$) for the removal of Co^{2+} ions from synthetic wastewater: kinetic, equilibrium and thermodynamic studies, Appl. Surf. Sci., 338 (2015) 42–54.

[12] D.H.K. Reddy, S.M. Lee, Three-dimensional porous spinel ferrite as an adsorbent for Pb(II) removal from aqueous solutions, Ind. Eng. Chem. Res., 52(2013) 15789–15800.

[13] L.P. Lingamdinne, I.S. Kim, J.H. Ha, Y.Y. Chang, J.R. Koduru, J.K. Yang, Enhanced adsorption removal of Pb (II) and Cr (III) by using nickel ferrite-reduced graphene oxide nanocomposite, Metals, 7 (2017) 225–240.

[14] A. Sengupta, R. Rao, D. Bahadur, Zn^{2+}–silica modified cobalt ferrite magnetic nanostructured composite for efficient adsorption of cationic pollutants from water, ACS Sustain. Chem. Eng., 5 (2017) 1280–1286.

[15] S. Rajput, C.U.P.J. Pittman, D. Mohan, Magnetic magnetite (Fe_3O_4) nanoparticle synthesis and applications for lead (Pb^{2+}) and chromium (Cr^{6+}) removal from water, J. Colloid Interface Sci., 468 (2016) 334–346.

[16] S. Mohan, V. Kumar, D.K. Singh, S.H. Hasan, Effective removal of lead ions using graphene oxide-MgO nanohybrid from aqueous solution: isotherm, kinetic and thermodynamic modeling of adsorption, J. Environ. Chem. Eng., 5 (2017) 2259–2273.

[17] S. Rajput, L.P. Singh, C.U. Pittman Jr., D. Mohan, Lead (Pb^{2+}) and copper (Cu^{2+}) remediation from water using superparamagnetic maghemite (γ-Fe_2O_3) nanoparticles synthesized by flame spray pyrolysis (FSP), J. Colloid Interface Sci., 492 (2017) 176–190.

[18] R. Ravindranath, P. Roy, A.P. Periasamy, Y.W. Chen, C.T. Liang, H.T. Chang, Fe_2O_3/Al_2O_3 microboxes for efficient removal of heavy metal ions, New J. Chem., 41 (2017) 7751–7757.

[19] J.A. Ramos Guivar, E. Sadrollahi, D. Menzel, E.G. Ramos Fernandes, E.O. López, M.M. Torres, J.M. Arsuaga, A. Arencibia, F.J. Litterst, Magnetic, structural and surface properties of functionalized maghemite nanoparticles for copper and lead adsorption, RSC Adv., 7 (2017) 28763–28779.

[20] R. Nagarajah, K.T. Wong, G. Lee, K.H. Chu, Y. Yoon, N.C. Kim, M. Jang, Synthesis of a unique nanostructured magnesium oxide coated magnetite cluster composite and its application for the removal of selected heavy metals, Sep. Purif. Technol., 174 (2017) 290–300.

[21] D.J. Kang, X.L. Yu, M.F. Ge, W.G. Song, One-step fabrication and characterization of hierarchical $MgFe_2O_4$ microspheres and their application for lead removal, Micropor. Mesopor. Mater., 207 (2015) 170–178.

[22] M.S. Mostafa, A.-S.A. Bakr, A.M.A. El Naggar, E.-S.A. Sultan, Water decontamination via the removal of Pb (II) using a new generation of highly energetic surface nano-material: $Co^{+2}Mo^{+6}$ LDH, J. Colloid Interface Sci., 461 (2016) 261–272.

[23] G.B.B. Varadwaj, O.A. Oyetade, S. Rana, B.S. Martincigh, S.B. Jonnalagadda, V.O. Nyamori, Facile synthesis of three-dimensional Mg–Al layered double hydroxide/partially reduced graphene oxide nanocomposites for the effective removal of Pb^{2+} from aqueous solution, ACS Appl. Mater. Interfaces, 9 (2017) 17290–17305.

[24] S.Q. Zhang, W.G. Hou, Sorption removal of Pb(II) from solution by uncalcined and calcined MgAl-layered double hydroxides, Chin. J. Chem., 25 (2007) 1455–1460.

[25] F.R. Zhang, N. Du, H.P. Li, X.F. Liang, W.G. Hou, Sorption of Cr(VI) on Mg–Al–Fe layered double hydroxides synthesized by a mechanochemical method, RSC Adv., 4 (2014) 46823–46830.

[26] X.F. Liang, W.G. Hou, J. Xu, Sorption of Pb(II) on Mg-Fe layered double hydroxide, Chin. J. Chem., 27 (2009) 1981–1988.

[27] X.F. Liang, W.G. Hou, Y.M. Xu, G.H. Sun, L. Wang, Y. Sun, X. Qin, Sorption of lead ion by layered double hydroxide intercalated with diethylenetriaminepentaacetic acid, Colloids Surf. A, 366 (2010) 50–57.

[28] L.L. Xiao, W. Ma, M. Han, Z.H. Cheng, The influence of ferric iron in calcined nano-Mg/Al hydrotalcite on adsorption of Cr (VI) from aqueous solution, J. Hazard. Mater., 186 (2011) 690–698.

[29] X.F. Liang, Y.B. Zang, Y.M. Xu, X. Tan, W.G. Hou, L. Wang, Y.B. Sun, Sorption of metal cations on layered double hydroxides, Colloids Surf. A, 433 (2013) 122–131.

[30] L.L. Ling, W.J. Liu, S. Zhang, H. Jiang, Achieving high-efficiency and ultrafast removal of Pb(II) by one-pot incorporation of a N-doped carbon hydrogel into FeMg layered double hydroxides, J. Mater. Chem. A, 4 (2016) 10336–10344.

[31] J.M. Gong, T. Liu, X.Q. Wang, X.L. Hu, L.Z. Zhang, Efficient removal of heavy metal ions from aqueous systems with the assembly of anisotropic layered double hydroxide nanocrystals@carbon nanosphere, Environ. Sci. Technol., 45 (2011) 6181–6187.

[32] W.Q. Chen, J.L. Xing, Z.H. Lu, J. Wang, S.J. Yu, W. Yao, A.M. Asiri, K.A. Alamry, X.K. Wang, S.H. Wang, Citrate-modified Mg-Al layered double hydroxides for efficient removal of lead from water, Environ. Chem. Lett., 16 (2018) 561–567.

[33] J. Yu, Z.L. Zhu, H. Zhang, Y.L. Qiu, D.Q. Yin, Mg-Fe layered double hydroxide assembled on biochar derived from rice husk ash: facile synthesis and application in efficient removal of heavy metals, Environ. Sci. Pollut. Res., 25 (2018) 24293–24304.

[34] M.F. Hansen, C.B. Koch, S. Mørup, Magnetic dynamics of weakly and strongly interacting hematite nanoparticles, Phys. Rev. B, 62 (2000) 1124–1135.

[35] Q. Wang, H.H. Tay, D.J.W. Ng, L.W. Chen, Y. Liu, J. Chang, Z.Y. Zhong, J.Z. Luo, A. Borgna, The effect of trivalent cations on the performance of Mg-M-CO_3 layered double hydroxides for high-temperature CO_2 capture, Chem. Sus. Chem., 3 (2010) 965–973.

[36] R. Elmoubarki, F.Z. Mahjoubi, A. Elhalil, H. Tounsadi, M. Abdennouri, M. Sadiq, S. Qourzal, A. Zpuhri, N. Barka, Ni/Fe and Mg/Fe layered double hydroxide s and their calcined derivatives: preparation, characterization and application on textile dyes removal, J. Mater. Res. Technol., 6 (2017) 271–283.

[37] H. Pfeiffer, E. Lima, V. Lara, J.S. Valente, Thermokinetic study of the rehydration process of a calcined MgAl-layered double hydroxide, Langmuir, 26 (2010) 4074–4079.
[38] D.A. Torres-Rodriguez, E. Lima, J.S. Valente, H. Pfeiffer, CO_2 capture at low temperatures (30–80°C) and in the presence of water vapor over a thermally activated Mg–Al layered double hydroxide, J. Phys. Chem. A, 115 (2011) 12243–12250.
[39] T. Kameda, S. Saito, Y. Umetsu, Mg-Al layered double hydroxide intercalated with ethylene-diaminetetraacetate anion: synthesis and application to the uptake of heavy metal ions from an aqueous solution, Sep. Purif. Technol., 47 (2005) 20–26.

Supplementary Information

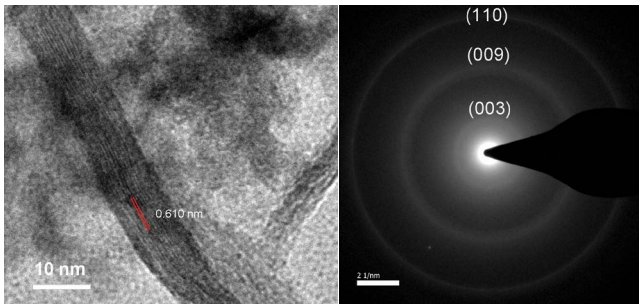

Fig. S1. HRTEM and SAED of MF400.

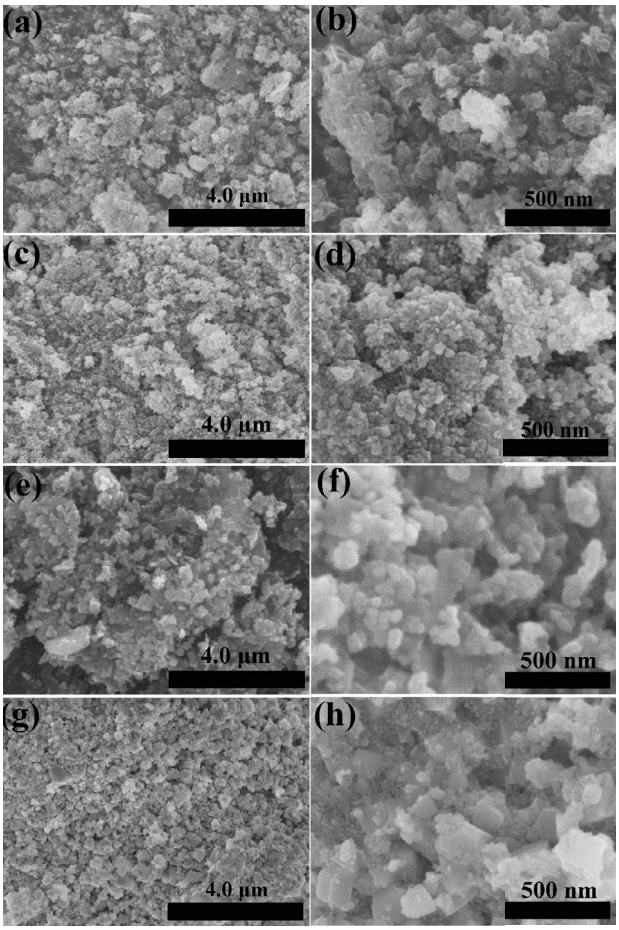

Fig. S2 SEM images at different magnification levels of MgFe compounds calcinated at different temperature: MF400 (a, b), MF600 (c, d), MF700 (e, f) and MF 800 (g, h).

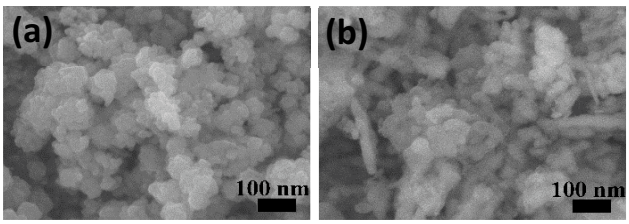

Fig. S3. SEM images of (a) Fe_2O_3 and (b) MgO.

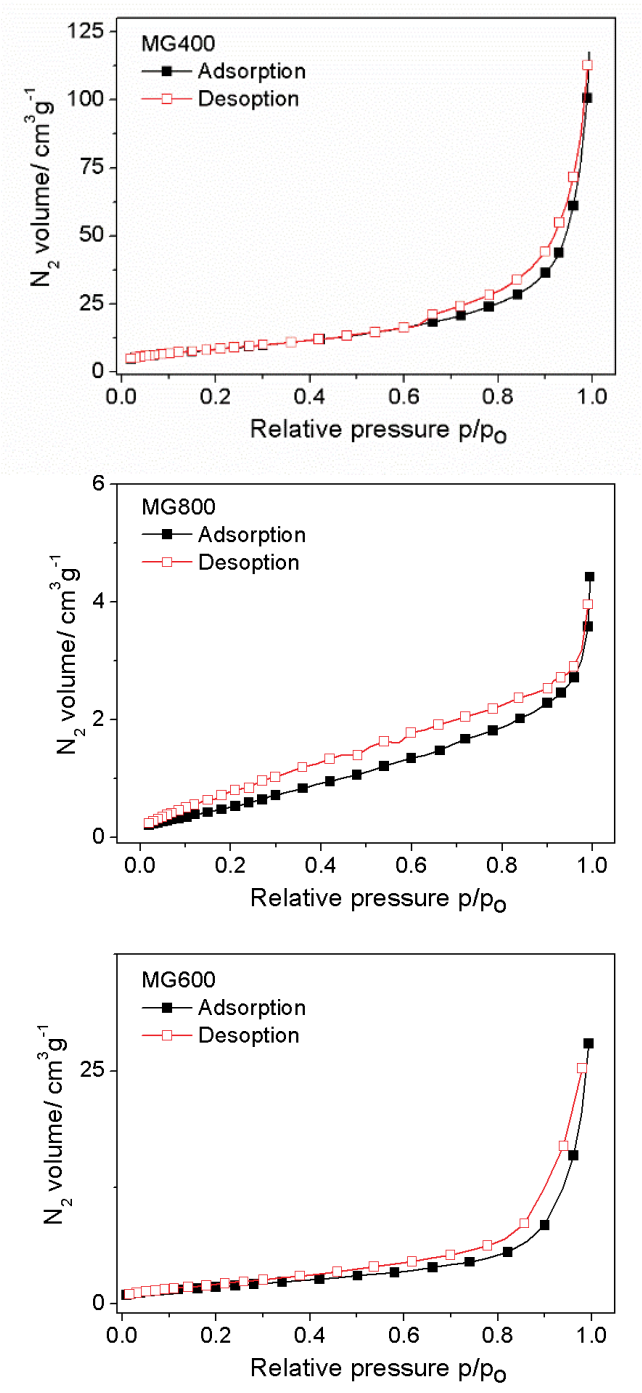

Fig. S4. N_2 isotherms for different samples.

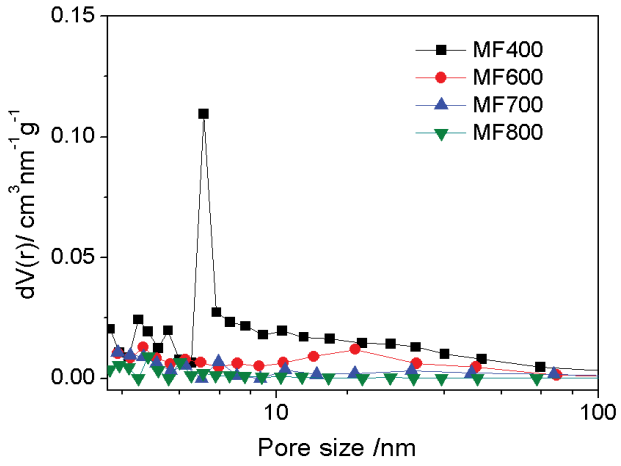

Fig. S5. Pore size distribution of different samples.

Table S1. Summary of N2 isotherm analysis.

	Surface area (m^2/g)	Pore volume (cm^3/g)	Pore size (nm)
MF400	185.62	1.091	5.95
MF600	65.46	0.420	N/A
MF700	34.17	0.267	N/A
MF800	12.79	0.038	N/A

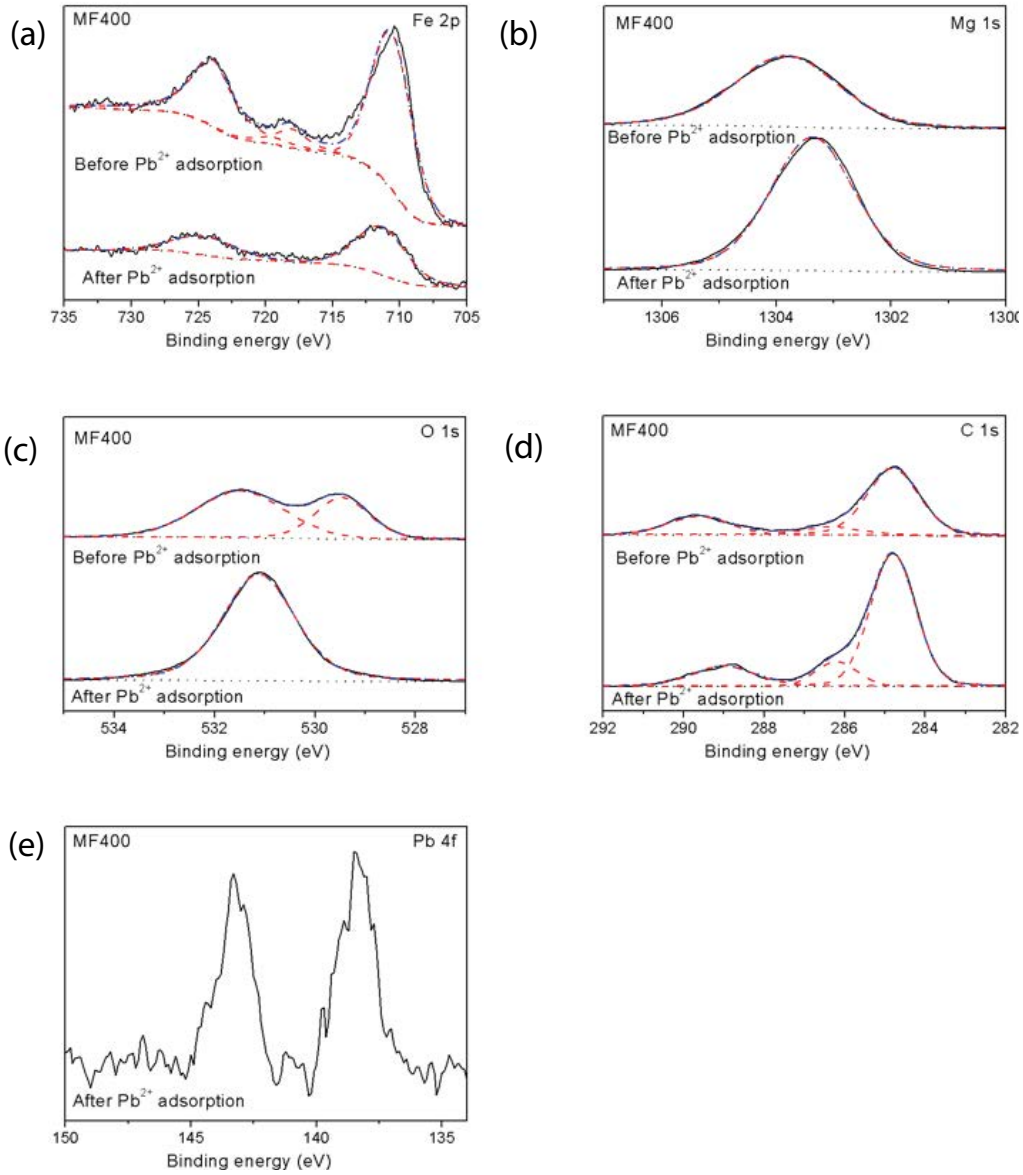

Fig. S6. XPS spectra of MF400 samples (a) Fe 2p(b) Mg 1s (c) O 1s (d) C 1s before and after lead adsorption; (e) Pb 4f after lead adsorption.

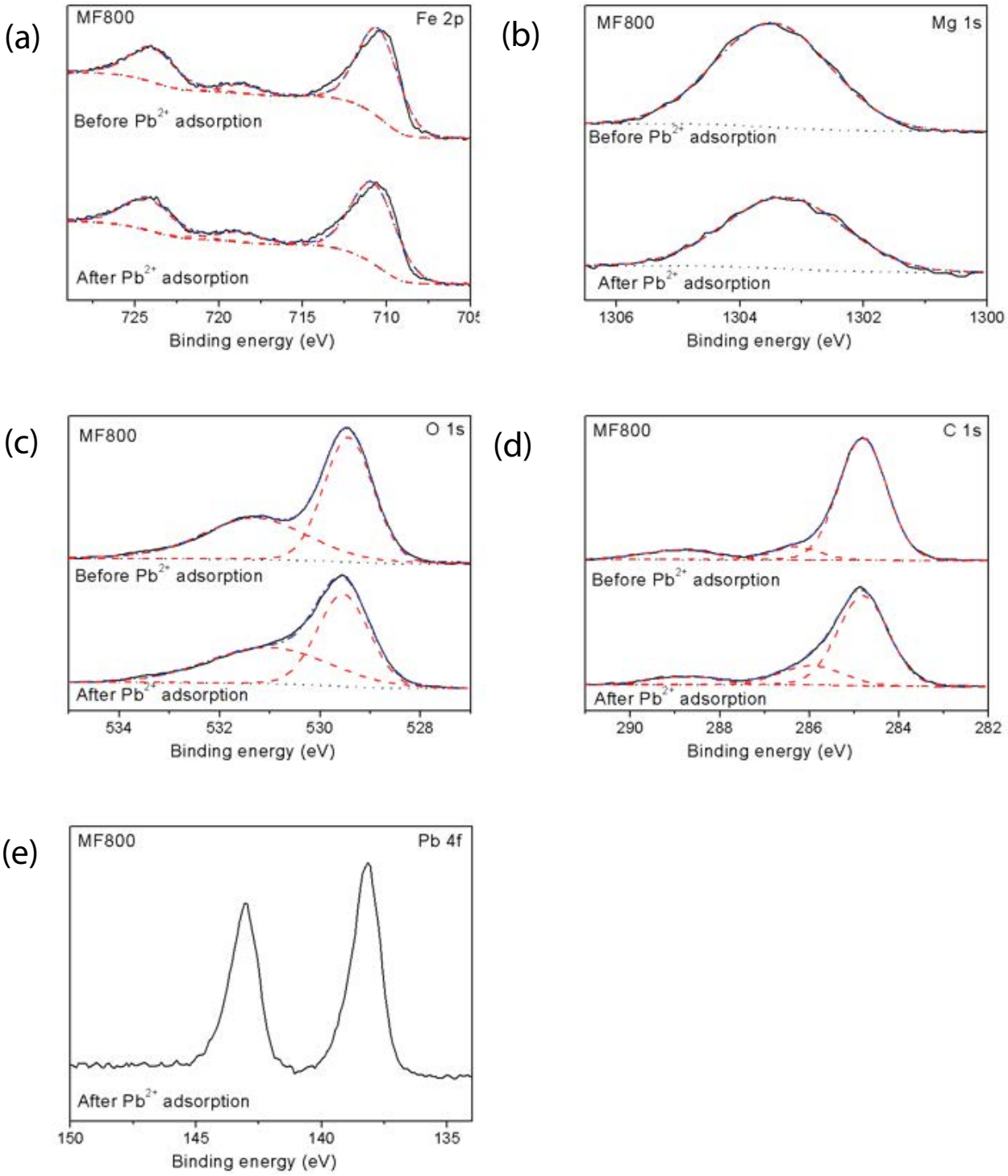

Fig. S7. XPS spectra of MF800 samples (a) Fe 2p (b) Mg 1s (c) O 1s (d) C 1s before and after lead adsorption; (e) Pb 4f after lead adsorption.